Electronic Supplementary Material (ESI) for CrystEngComm.
This journal is © The Royal Society of Chemistry 2020

Supporting Information

Mechanochemical approaches towards the *in situ* confinement of 5-FU anti-cancer drug within MIL-100 (Fe) metal-organic framework

Barbara E. Souza[a] and Jin-Chong Tan*[a]

[a]*Multifunctional Materials & Composites (MMC) Laboratory, Department of Engineering Science, University of Oxford, Parks Road, Oxford OX1 3PJ, UK*

**jin-chong.tan@eng.ox.ac.uk*

Table of Contents

1. Materials synthesis 2
  1.1. Mechanochemistry of MIL-100 (Fe) 2
  1.2. Fabrication of drug@MIL-100 systems *via in situ* encapsulation 2
2. Materials characterization 2
  1.3. Powder X-ray diffraction (PXRD) 2
  1.4. Thermogravimetric analysis (TGA) 3
  1.5. Attenuated total reflectance Fourier transform infrared spectroscopy (ATR-FTIR) 3
  1.6. Scanning electron microscopy (SEM) 3
  1.7. Specific surface area measurements 3
  1.8. Calculation of PXRD peaks height and full width at half maximum of ATR-FTIR peaks .. 3
  1.9. Drug release experiments 3
  1.10. Density function theory (DFT) calculations and proton acceptor/donor sites determination4
3. Results 5
3.1. MIL-100 (Fe) diffraction data 5
3.2. 5-Fluorouracil (5-FU) molecular vibrations 7
3.3. SEM images for morphological characterization 9
3.4. Textural properties of MIL-100 (Fe) samples 10
3.5. Thermal properties of MIL-100 (Fe) samples 10
3.6. Fitted curves of drug release profiles 11
3.7. MIL-100 (Fe) stability during drug release experiments 12

1. Materials synthesis

1.1. Mechanochemistry of MIL-100 (Fe)

Two different mechanochemical-annealing approaches were used towards the fabrication of pristine MIL-100 (Fe) material. First, MIL-100 (Fe) manually ground (MG) was synthesized *via* a manual mechanochemistry process. $Fe(NO_3)\cdot 9H_2O$ [iron(III) nitrate 9-hydrate] (3 mmol) and H_3BTC [benzene-1,3,5-tricarboxilic acid] (2 mmol) were combined in the agate mortar and manually ground for 10 min.

Secondly, for the synthesis of MIL-100 vortex ground (VG) sample a similar procedure was followed. The same amounts of initial reactants were placed in a polypropylene tube (ø 23 mm × 85 mm) together with three Ø4 mm stainless steel spheres (ball bearings). The tube was covered with a lid and secured to a standard IKA Mixer Vortex Shaker using a 3D-printed holder and then agitated at 1200 rpm for 10 min.

The resulting material from both grinding processes was placed in an autoclave flask and kept in oven at 160 °C for 4 h, to complete the annealing process. The product was washed by centrifugation (8000 rpm for 10 min) with methanol to remove any unreacted components. Pristine MIL-100 (Fe) was then dried at room temperature and activated under vacuum at 150 °C for 12 h.

1.2. Fabrication of drug@MIL-100 systems *via in situ* encapsulation

Two guest@MOF composite samples were synthesized as follows. For the (one-pot) *in situ* encapsulation of 5-FU, analogous procedure was followed to the fabrication of pristine MIL-100 (Fe) with the addition of 3.0 mmol of 5-FU during the grinding process, producing the 5-FU@MIL-100_MG particles *via* manual grinding and 5-FU@MIL-100_VG particles *via* vortex grinding. The drug-loaded samples were washed by centrifugation (8000 rpm for 10 min) with methanol and then activated at 150 °C for 12 h in a vacuum oven. The amount of 5-FU used was selected to maintain a 2:3 molecular ratio of H_3BTC:5-FU to maximize the deprotonation of the organic ligand by the drug molecules and to favour the formation of a highly crystalline host framework (as discussed in the main text).

Table S1: Samples description and details

	Sample	Synthesis method
1	MIL-100 (Fe) MG	Manual grinding-annealing
2	MIL-100 (Fe) VG	Vortex grinding-annealing
3	5-FU@MIL-100_MG	*In situ* manual grinding encapsulation
4	5-FU@MIL-100_VG	*In situ* vortex grinding encapsulation
5	5-Fluorouracil (5-FU)*	-

*Used as-received

2. Materials characterization

1.3. Powder X-ray diffraction (PXRD)

The powder samples were analyzed by PXRD using the Rigaku MiniFlex diffractometer with a Cu K_α source (1.541 Å). Diffraction data were collected from 3° to 13°, using a 0.02° step size and 0.1° min^{-1} step speed. The patterns were then normalized with respect to the most intense peak (plane (022)) in the pattern [0-1]. Raw PXRD data were used for the calculation of peaks broadening/sharpening to minimize effects of background subtraction and data normalization.

1.4. Thermogravimetric analysis (TGA)

TGA was performed using TGA-Q50 (TA instruments). Approximately 4 mg of each sample were placed in a platinum pan (maximum volume 50 µL) and heated from 50 °C to 500 °C with a heating rate of 10 °C min^{-1}. The measurements were performed under a dry nitrogen flow of 40 mL min^{-1}.

1.5. Attenuated total reflectance Fourier transform infrared spectroscopy (ATR-FTIR)

ATR-FTIR spectra were acquired at room temperature with a Nicolet iS10 FTIR spectrometer with an ATR sample holder. The spectra were collected in the range of 650-2000 cm^{-1} with a resolution of 4 cm^{-1} and normalized in respect to the most intense vibrational peak to facilitate comparison across the different samples under study.

1.6. Scanning electron microscopy (SEM)

Analyses of the morphology and particle size determination were carried out by SEM, which were obtained using Carl Zeiss EVO LS15 at 15 keV under high vacuum.

1.7. Specific surface area measurements

The Brunauer-Emmett-Teller (BET) specific surface area of samples was determined from nitrogen adsorption isotherms at 77 K, measured with Quantachrome Nova 1200. The isotherms were obtained using a Ø9 mm sample cell containing 60-100 mg of the samples under study. The outgassing temperature was 150 °C during sample activation under vacuum overnight.

1.8. Calculation of PXRD peaks height and full width at half maximum of ATR-FTIR peaks

The Integrate Gadget in OriginPro software was used to perform the numerical integration on the PXRD patterns and determine the full width at half maximum (FWHM) of two of the most intense diffraction peaks in the MIL-100 (Fe) samples (i.e. $2\theta = 4°$ and 11°) that correspond to the (022) and (357) planes respectively. The range of data was selected to include the peaks of the diffraction pattern of interest, using the (horizontal) diffraction angle axis as the baseline. To facilitate the comparison between the effect of the reconstruction process, the ratio between the peak heights, i.e. (022):(357) was taken and the FWHM values were normalized against the largest value presented within a set of samples.

1.9. Drug release experiments

5-FU release experiments were carried out at 37 °C with magnetic agitation, using phosphate buffered saline (PBS, 0.04 M pH 7.4) to simulate physiological conditions. 10 mg of the drug-loaded samples were immersed in 5 mL of PBS. At different incubation times, 1 mL of supernatant was recovered by centrifugation and replaced with the same volume of fresh PBS at 37 °C. The amount of 5-FU released was determined by UV-Vis spectroscopy at 266 nm. The accurate concentration of 5-FU released was determined using the calibration curve expressed in Equation (1), which was constructed by correlating the absorbance and concentration of various measured 5-FU solutions.

$$A = 0.05275. c \qquad (1)$$

where A is the measured absorbance and the c the concentration (in μg/mL) of the collected aliquot.

1.10. Density function theory (DFT) calculations and proton acceptor/donor sites determination

DFT calculations to generate the vibrational spectrum of 5-FU were performed using the Gaussian software.[1] The vibrational calculations were carried out at the B3LYP level of theory and 6-31G basis set. The proton acceptor/donor sites present in the guest drug molecule were determined using BIOVIA Discovery Studio.

3. Results

3.1. MIL-100 (Fe) diffraction data

The FWHM values were normalized against the largest value presented within a set of samples in order to facilitate the comparison of the effect of the guest encapsulation on the different samples. Fig. S1a shows that 5-FU encapsulated samples have a relatively sharper (022) peak. This is due to the role played by 5-FU proton acceptor sites (Fig. S1b), which aid the deprotonation of the H_3BTC organic linkers hence resulting in samples with improved crystallinity.

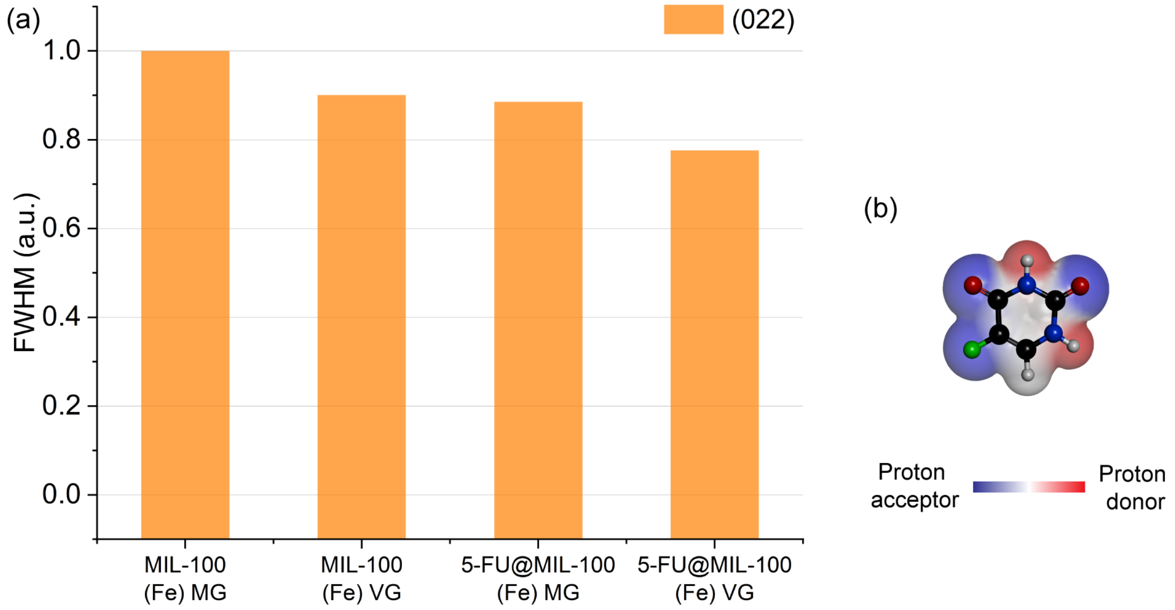

Fig. S1 (a) FWHM values of (022) peak of MIL-100 (Fe) MG and MIL-100 (Fe) VG and their drug-loaded counterparts. (b) Schematic representation of 5-FU molecules showing the proton acceptor and donor sites. Colour code: O in red, C in black, H in grey, N in navy blue, and F in green.

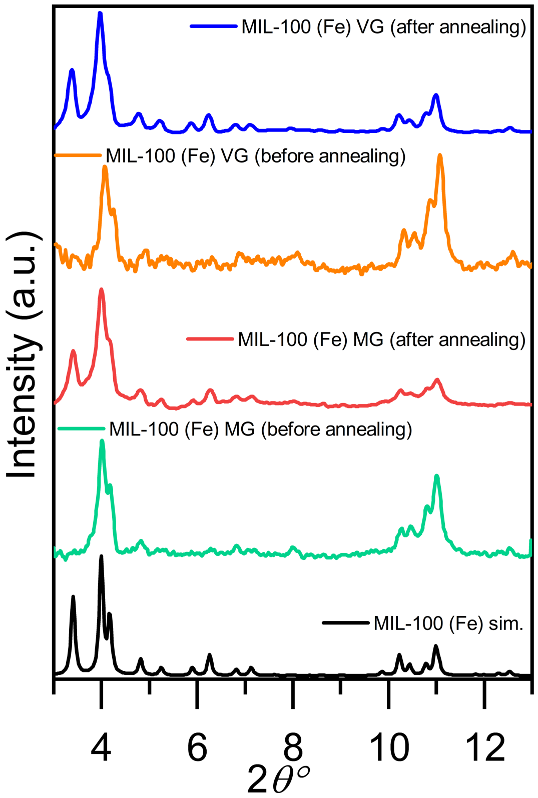

Fig. S2 PXRD patterns of MIL-100 (Fe) before and after the annealing step after the mechanochemical grinding (MG and VG) process. The contrast between the patterns before and after annealing for the manually and vortex ground samples revealed that the mechanical stress (from grinding) have resulted in framework formation prior to the annealing step. Annealing is therefore used to enhance material crystallinity.

3.2. 5-Fluorouracil (5-FU) molecular vibrations

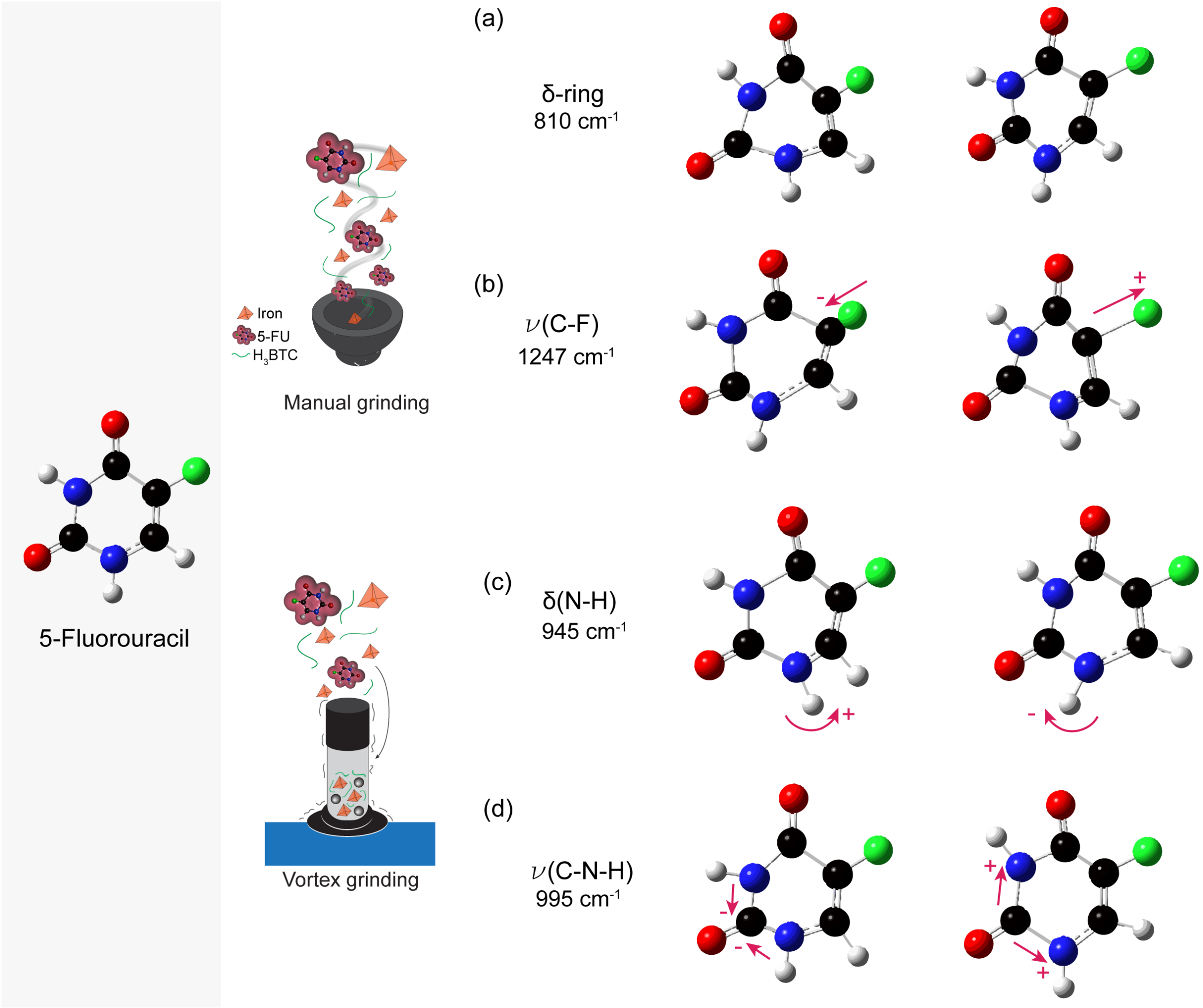

Fig. S3 Schematic representation of the molecular vibrational modes of 5-FU at different wavenumbers. (a) Bending mode of the uracil ring. (b) Stretching of C-F bond. (c) Bending of N-H bond. (d) Stretching C-N-H bonds.

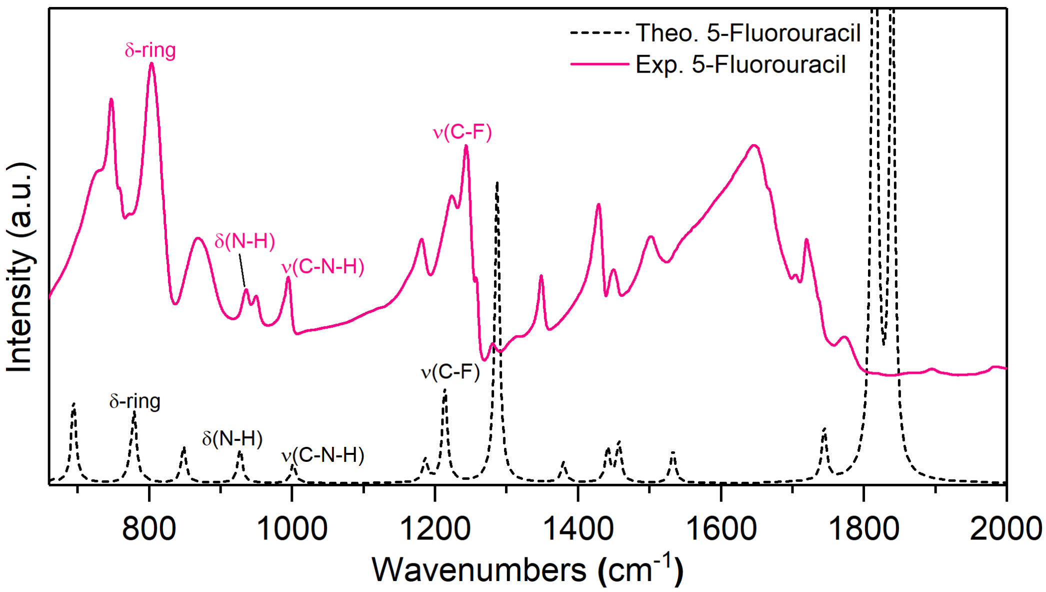

Fig. S4 Comparison between theoretical and experimental vibrational spectra of 5-FU used to identify the specific vibrational modes marked in the plot. A reasonably good match between the experimental and theoretical spectra was observed, where the mismatch between the theoretical and experimental frequencies is a common shift resulting from the *ab initio* calculations.[2]

3.3. SEM images for morphological characterization

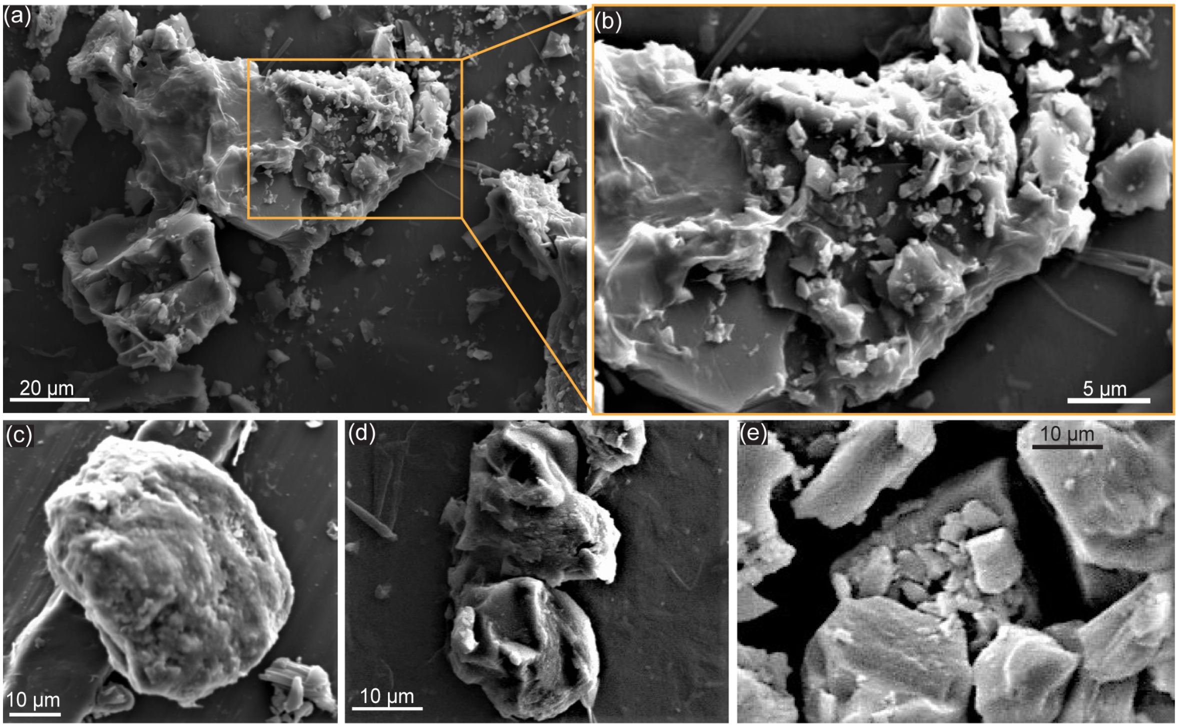

Fig. S5 SEM images of as-synthesized (a-b) MIL-100 (Fe) MG, (c-e) MIL-100 (Fe) VG. The micrographs display a non-uniform particle distribution, due to the grinding nature of the synthesis method.

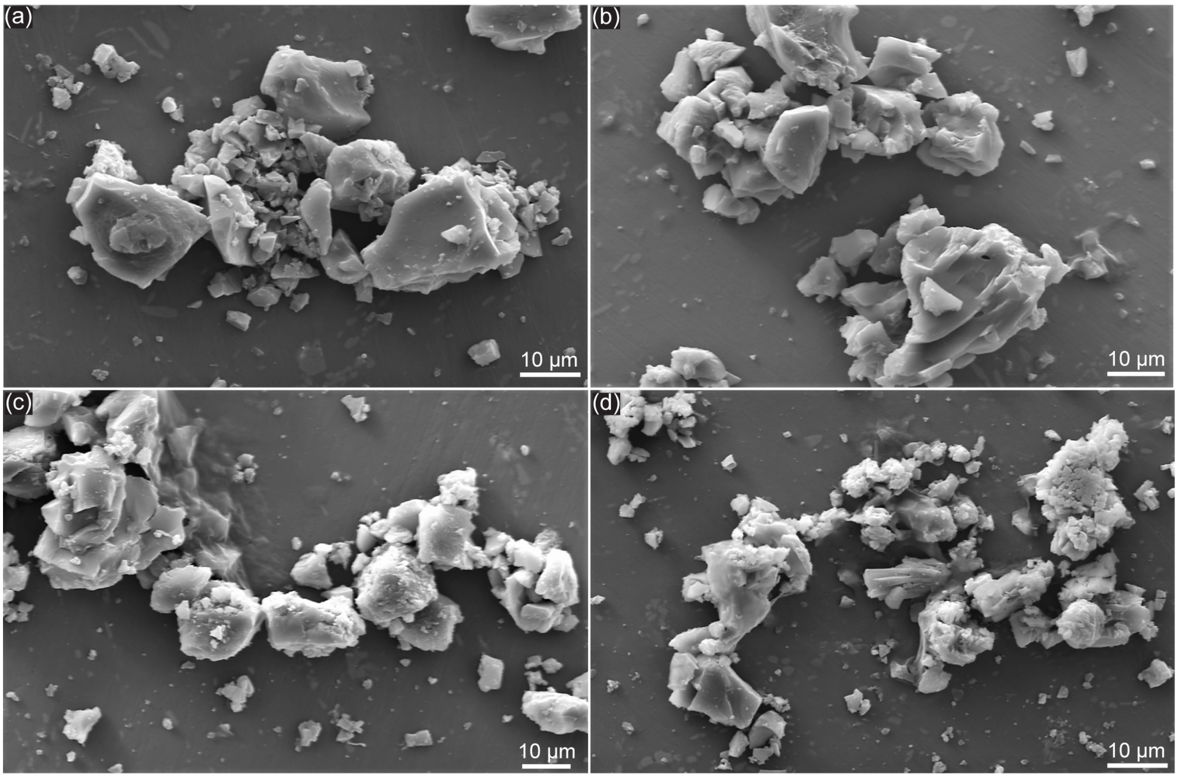

Fig. S6 SEM images comparing as-synthesized (a) MIL-100 (Fe) MG, (b) MIL-100 (Fe) VG, and drug-loaded (c) 5-FU@MIL-100_MG, and (d) 5-FU@MIL-100_VG. The micrographs display the absence of morphological changes upon drug encapsulation

3.4. Textural properties of MIL-100 (Fe) samples

Evaluation of the BET surface area of the pristine MIL-100 (Fe) MG and MIL-100 (Fe) VG samples, presented in Table S2, displays agreement with the values of other reported MIL-100 samples synthesized *via* conventional methods or by mechanochemistry.

Table S2. Comparison of textural properties of MIL-100 (Fe) samples produced *via* various methods

Sample	Synthesis method	BET surface area (m^2 g^{-1})	Reference
MIL-100 (Fe) MG	Manual grinding	793	This work
MIL-100 (Fe) VG	Vortex grinding	753	
5-FU@MIL-100_MG	Manual grinding	333	
5-FU@MIL-100_VG	Vortex grinding	697	
MIL-100 (Fe)	Mechanochemistry (high pressure and temperature)	1940	Han et al.[3]
	Mechanochemistry (Liquid assisted grinding - ball mill)	1033	Pilloni et al.[4]
	Mechanochemical (kitchen grinder)	255	Samal et al.[5]
	Solvothermal (high pressure and temperature)	1750	Chen et al.[6]
	Solvothermal (high pressure and temperature)	1223.32	Zhang et al.[7]
	Solid state synthesis (high pressure and temperature)	110.49	Chaturvedi et al.[8]

3.5. Thermal properties of MIL-100 (Fe) samples

Table S3 showcases in detail the decomposition process of MIL-100 (Fe) and drug@MOF samples acquired from thermogravimetric analysis. An increase in the initial decomposition temperature of 5-FU@MIL-100_MG and 5-FU@MIL-100_VG in comparison to MIL-100 (Fe) MG and MIL-100 (Fe) VG (increase of ~30 °C) was observed. An increase in the rate of decomposition between drug-loaded and pristine MIL-100 (Fe) host was noted. This corresponds to different decomposing amounts as a function of temperature due to the presence of the encapsulated guest molecules. The presence of the guest molecules is also reflected in the temperature at which half of the material has decomposed. Meanwhile, the final residue has presented very little change.

Table S3. Analysis of thermal decomposition of MIL-100 (Fe) samples

	Initial decomposition temperature	Maximum rate of decomposition	Temperature of half decomposition	Final residue (at 500 °C)
MIL-100 (Fe) MG	290 °C	-0.266 %/°C	331 °C	36.6%
MIL-100 (Fe) VG	290 °C	-0.238 %/°C	332 °C	34.6%
5-FU@MIL-100 (Fe) MG	320 °C	-0.429 %/°C	349 °C	32.6%
5-FU@MIL-100 (Fe) VG	321 °C	-0.403 %/°C	360 °C	38.2%

The drug loading was calculated from the TGA plots analysis *via* the formula:

$$\mathrm{wt.\%} = \frac{\mathrm{m_{loss\ (drug@MOF)}} - \mathrm{m_{loss\ (MOF)}}}{\mathrm{m_{loss\ (drug@MOF)}}}$$

where $\mathrm{m_{loss\ (drug@MOF)}}$ is the weight loss of the drug@MOF systems and $\mathrm{m_{loss\ (MOF)}}$ is the weight loss of the host MOF.

The drug loading was measured in the temperature range corresponding to the decomposition of 5-FU (180-330 ºC)

3.6. Fitted curves of drug release profiles

Table S4 shows the fitting equations and fitting parameters of the experimental release profiles of 5-FU@MIL-100_MG and 5-FU@MIL-100_VG. The profiles were fitted to a general hyperbola function with high coefficients of determination (R^2).

Table S4. Fit equations for the 5-FU drug release profiles, the fitted curves are shown in Fig. 3 of the main manuscript.

Sample	Equation	R^2
5-FU@MIL-100_MG	$5\text{-}FU(\%)_{MG} = 46.83 - \frac{158.00}{(1+41305.08 * t)^{\frac{1}{6.00}}}$	0.99121
5-FU@MIL-100_VG	$5\text{-}FU(\%)_{VG} = 64.02 - \frac{43.08}{(1+1.98 * t)^{\frac{1}{1.68}}}$	0.99364

3.7. MIL-100 (Fe) stability during drug release experiments

The initial assessment of the host stability of MIL-100 (Fe) during the time period of drug release experiments has been performed *via* analysis of UV-Vis spectrometry and PXRD patterns. The analysis of the PXRD patterns was performed as follows.

The Scherrer law allows one to determine the size of the crystalline domains *D*:[9]

$$D = \frac{K\lambda}{\Delta cos\theta}$$

where λ is the wavelength, Δ = FWHM, K is a constant, and θ is the diffraction angle of the corresponding diffraction peak.

As the samples might present different particle sizes and different packing configurations, the best representation to establish the cross comparison of such samples was the "crystallinity" defined as:

$$Crystallinity = \frac{D_{final}}{D_{initial}}$$

Then:

$$Crystallinity = \frac{\frac{K\lambda}{\Delta_{final} cos\theta}}{\frac{K\lambda}{\Delta_{initial} cos\theta}} = \frac{\Delta_{initial}}{\Delta_{final}}$$

As reflected by Fig. S5a, no apparent decomposition of the MIL-100 (Fe) host took place during the release experiments. Minor changes in the FWHM of the (022) peaks were observed (Fig. S5b), reflected by the change in the relative width of the peak (*i.e.* crystallinity). The minimal broadening of the (022) peak demonstrates the good retainment of the samples crystallinity.

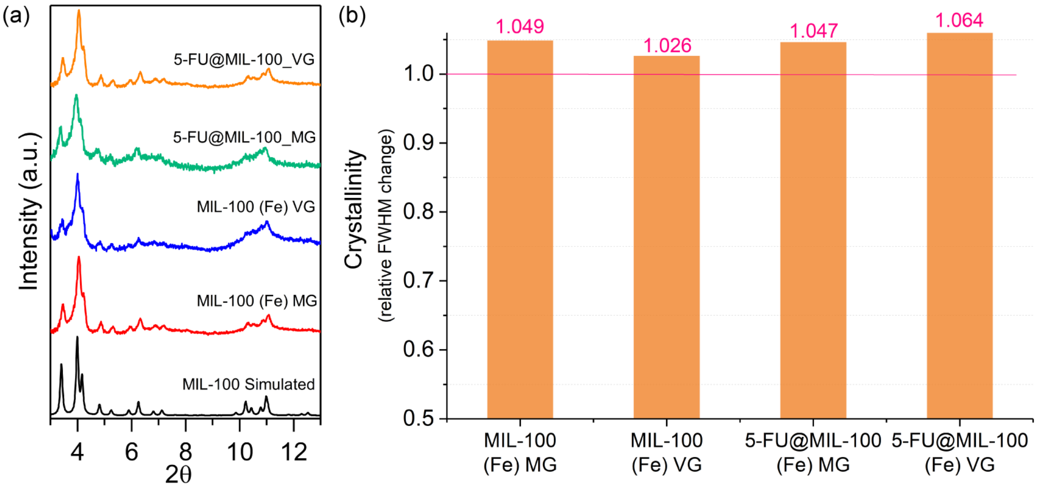

Fig. S7 Analysis of diffraction data of MIL-100 (Fe) samples after release experiments. (a) PXRD patterns of pristine MIL-100 (Fe) and drug-loaded samples, displaying that the materials hold good crystallinity after immersion in PBS during the release experiments. (b) Relative FWHM of samples, the ratio was taken in relation to the initial value for the FWHM of the samples before the release experiments.

The stability of the host framework was further assessed *via* UV-Vis spectroscopy. As shown in Fig. S6, MIL-100 (Fe) does not present strong absorbance in the spectral region where we find the characteristic 5-FU band at 266 nm, used for monitoring the drug release. No significant changes to the UV-Vis spectra of MIL-100 (Fe) were observed over a 72-hour period.

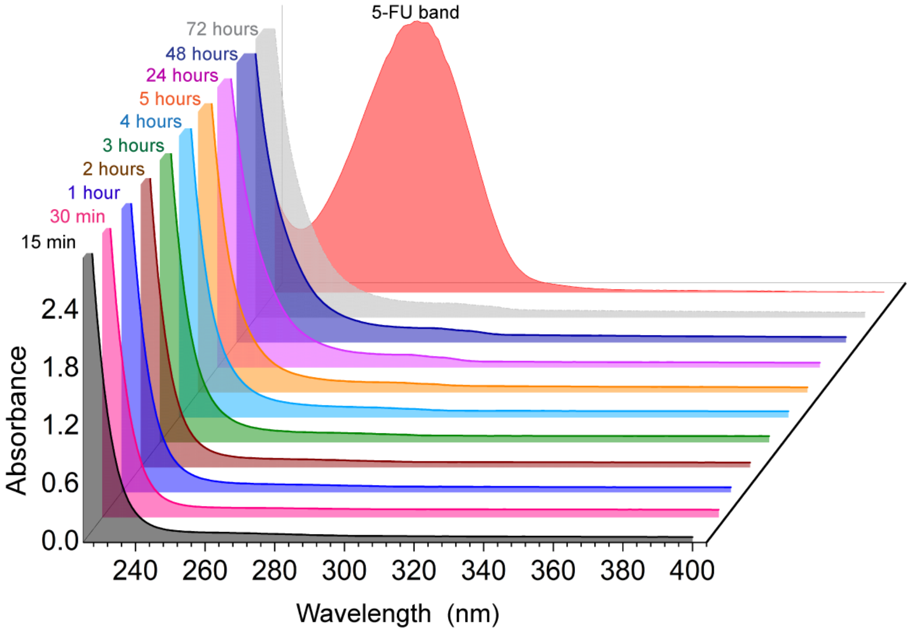

Fig. S8 UV-Vis spectra of the supernatant of MIL-100 (Fe) in PBS showing the good stability of MIL-100 (Fe) host during the release of 5-FU guest. The contrast with 5-FU spectrum (red trace) highlights the absence of any absorbance associated with decomposition of MIL-100 (Fe) that could interfere with the band at 266 nm used to track the release of 5-FU.

3.8. Manual grinding and vortex grinding applied to drug encapsulation

We acknowledge the limitations imposed by the manual grinding process herein utilized, specifically in terms of reproducibility. However, the advantages presented by this method and its simplicity (i.e. low associated cost and easy accessibility) could be exploited for the rapid fabrication of different guest@host systems in lab scale. Furthermore, manual grinding was employed as a comparison to the (more automated) vortex grinding method used in this study.

In manual grinding, the mechanical deformation induced is a result of the shear stress created in the regions of sliding contact between the pestle, reactants, and mortar. It creates a 2D distribution of the grinding force over a larger surface area, which might facilitate the improved formation of multiple MIL-100 secondary building units (SBU). Since the concept behind an *in situ* encapsulation technique is based on the host cages rapidly forming around the guest molecules, we believe that the multiplicity of SBU simultaneously and adjacently formed on the manual grinding process could explain the detected higher effectiveness of this method in achieving the confinement of 5-FU guest molecules. In contrast, for the vortex grinding process used in our setup (Fig. 1g), the simultaneous formation of adjacent SBU is expected to be relatively smaller due the reduced region of contact from the normal stress generated by the impact collision of stainless-steel balls. The results indicate that drug confinement is less effective for the latter process. A continuous shear stress is also present in twin-screw extrusion (TSE) methods, proven to be efficient for the fabrication of different MOF materials.[10]

The role played by a combination of different mechanical stresses coupled with time-dependent material response (e.g. rate-dependent viscous effects) should be the topics of future research to gain a better understanding and control of the mechanochemical process.

References

1. G. W. T. M. J. Frisch, H. B. Schlegel, G. E. Scuseria, M. A. Robb, J. R. Cheeseman, G. Scalmani, V. Barone, G. A. Petersson, H. Nakatsuji, X. Li, M. Caricato, A. Marenich, J. Bloino, B. G. Janesko, R. Gomperts, B. Mennucci, H. P. Hratchian, J. V. Ortiz, A. F. Izmaylov, J. L. Sonnenberg, D. Williams-Young, F. Ding, F. Lipparini, F. Egidi, J. Goings, B. Peng, A. Petrone, T. Henderson, D. Ranasinghe, V. G. Zakrzewski, J. Gao, N. Rega, G. Zheng, W. Liang, M. Hada, M. Ehara, K. Toyota, R. Fukuda, J. Hasegawa, M. Ishida, T. Nakajima, Y. Honda, O. Kitao, H. Nakai, T. Vreven, K. Throssell, J. A. Montgomery, Jr., J. E. Peralta, F. Ogliaro, M. Bearpark, J. J. Heyd, E. Brothers, K. N. Kudin, V. N. Staroverov, T. Keith, R. Kobayashi, J. Normand, K. Raghavachari, A. Rendell, J. C. Burant, S. S. Iyengar, J. Tomasi, M. Cossi, J. M. Millam, M. Klene, C. Adamo, R. Cammi, J. W. Ochterski, R. L. Martin, K. Morokuma, O. Farkas, J. B. Foresman, and D. J. Fox, *Gaussian, Inc.,*, 2016.
2. H. Matsuura, H. Yoshida and J. M. Chalmers, in *Handbook of Vibrational Spectroscopy*, John Wiley & Sons, Chichester, 2006.
3. L. Han, H. Qi, D. Zhang, G. Ye, W. Zhou, C. M. Hou, W. Xu and Y. Y. Sun, *New J. Chem.*, 2017, **41**, 13504-13509.
4. M. Pilloni, F. Padella, G. Ennas, S. Lai, M. Bellusci, E. Rombi, F. Sini, M. Pentimalli, C. Delitala, A. Scano, V. Cabras and I. Ferino, *Microporous Mesoporous Mat.*, 2015, **213**, 14-21.
5. M. Samal, J. Panda, B. P. Biswal and R. Sahu, *CrystEngComm*, 2018, **20**, 2486-2490.
6. G. Chen, X. Leng, J. Luo, L. You, C. Qu, X. Dong, H. Huang, X. Yin and J. Ni, *Molecules*, 2019, **24**.
7. X. Zhang, Q. Shi, B. Shen, Z. Hu and X. Zhang, *J. Hazard Mater.*, 2019, **381**, 121003.
8. G. Chaturvedi, A. Kaur, A. Umar, M. A. Khan, H. Algarni and S. K. Kansal, *J. Solid State Chem.*, 2020, **281**.
9. V. Guillerm, F. Ragon, M. Dan-Hardi, T. Devic, M. Vishnuvarthan, B. Campo, A. Vimont, G. Clet, Q. Yang, G. Maurin, G. Ferey, A. Vittadini, S. Gross and C. Serre, *Angew. Chem. Int. Ed.*, 2012, **51**, 9267-9271.
10. D. E. Crawford, C. K. G. Miskimmin, A. B. Albadarin, G. Walker, S. L. James, *Green Chem.,* 2017, **19**, 1507-1518.